Featured in Physics

Merger and Postmerger of Binary Neutron Stars with a Quark-Hadron Crossover Equation of State

Yong-Jia Huang,[1,2,3,*] Luca Baiotti,[4] Toru Kojo,[5,6] Kentaro Takami,[7,3] Hajime Sotani,[8,3] Hajime Togashi,[6] Tetsuo Hatsuda,[3] Shigehiro Nagataki,[3,8] and Yi-Zhong Fan[1,2]

[1]*Key Laboratory of Dark Matter and Space Astronomy, Purple Mountain Observatory, Chinese Academy of Science, Nanjing 210023, China*

[2]*School of Astronomy and Space Sciences, University of Science and Technology of China, Hefei, Anhui 230026, China*

[3]*RIKEN Interdisciplinary Theoretical and Mathematical Sciences Program (iTHEMS), RIKEN, Wako 351-0198, Japan*

[4]*International College and Graduate School of Science, Osaka University, 1-2 Machikaneyama-cho, Toyonaka, Osaka 560-0043, Japan*

[5]*Key Laboratory of Quark and Lepton Physics (MOE) and Institute of Particle Physics, Central China Normal University, Wuhan 430079, China*

[6]*Department of Physics, Tohoku University, Sendai 980-8578, Japan*

[7]*Kobe City College of Technology, 651-2194 Kobe, Japan*

[8]*RIKEN Astrophysical Big Bang Laboratory (ABBL), Cluster for Pioneering Research, Wako, Saitama 351-0198, Japan*

(Received 9 March 2022; revised 21 August 2022; accepted 19 September 2022; published 26 October 2022)

Fully general-relativistic binary-neutron-star (BNS) merger simulations with quark-hadron crossover (QHC) equations of state (EOS) are studied for the first time. In contrast to EOS with purely hadronic matter or with a first-order quark-hadron phase transition (1PT), in the transition region QHC EOS show a peak in sound speed and thus a stiffening. We study the effects of such stiffening in the merger and postmerger gravitational (GW) signals. Through simulations in the binary-mass range $2.5 < M/M_\odot < 2.75$, characteristic differences due to different EOS appear in the frequency of the main peak of the postmerger GW spectrum (f_2), extracted through Bayesian inference. In particular, we found that (i) for lower-mass binaries, since the maximum baryon number density ($n_{\max}$) after the merger stays below 3–4 times the nuclear-matter density (n_0), the characteristic stiffening of the QHC models in that density range results in a lower f_2 than that computed for the underlying hadronic EOS and thus also than that for EOS with a 1PT; (ii) for higher-mass binaries, where $n_{\max}$ may exceed 4–$5n_0$ depending on the EOS model, whether f_2 in QHC models is higher or lower than that in the underlying hadronic model depends on the height of the sound-speed peak. Comparing the values of f_2 for different EOS and BNS masses gives important clues on how to discriminate different types of quark dynamics in the high-density end of EOS and is relevant to future kilohertz GW observations with third-generation GW detectors.

DOI: 10.1103/PhysRevLett.129.181101

Introduction.—Multimessenger astronomy, including gravitational, electromagnetic, and neutrino signals, has started offering new ways of obtaining information on ultrahigh-density matter [1]. Observations of the inspiral of a binary-neutron-star (BNS) merger may provide information on the equation of state (EOS) at a few times the nuclear saturation number density ($n_0 = 0.16\ \mathrm{fm}^{-3}$), and even higher densities (several times n_0) may be investigated through observations of the postmerger phase, where matter is also hotter than in the inspiraling neutron stars (NSs) [2,3]. In the near future, the detection of BNS mergers will happen on a daily basis and this will also allow one to perform improved statistical analyses of the properties of their EOS.

The EOS plays a crucial role in determining the structure of NSs. See Fig. 1 for schematic plots of the mass-radius and energy-pressure relations in NSs with different types of EOS. Nuclear EOS based on microscopic nuclear two- and three-body forces are supposed to be valid up to number densities $n \simeq 1.5$–$2n_0$ and thus to describe somewhat accurately the equatorial radii of canonical NSs (mass $M \simeq 1.4\ M_\odot$), which have core densities around 2–$3n_0$. The most massive NS known, PSR J0740 + 6620, has mass $M/M_\odot = 2.08 \pm 0.07$ [4] and inferred core density $\gtrsim 3$–$4n_0$. This is close to the density at which baryons with radii $\simeq$0.5–0.8 fm begin to overlap, presumably resulting in matter beyond the purely hadronic regime, such as quark matter.

One of the fundamental questions in the study of ultradense matter is how the quark-hadron phase transition takes place. The most intensively studied scenario is the one involving first-order quark-hadron phase transitions (1PTs). In this case, it is usually believed that pressure support (and thus the radius of the material object resulting from the merger) decreases abruptly after the phase transition. Such a change in compactness would appear,

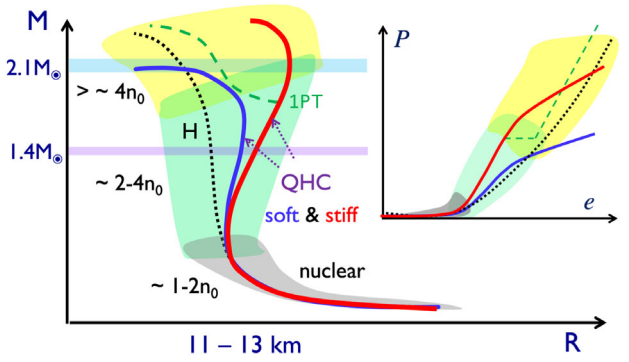

FIG. 1. Schematic plots for the (main figure) mass-radius relations and (inset) pressure P vs energy density e for some EOS satisfying constraints from terrestrial experiments and the observational fact that a NS of mass $\approx 2\ M_\odot$ exists; H refers to a purely hadronic model, 1PT to a hybrid model with a first-order quark-hadron phase transition, and QHC to models with a quark-hadron crossover. QHC models show stiffening at densities lower than in the other two cases, typically leading to larger radii and smaller central densities for NSs with masses 1.4–2 $M_\odot$. The gray, green, and yellow shaded areas in both the main figure and inset correspond to the number density ranges of $n \sim 1$–$2n_0$, $\sim$2–$4n_0$, and $\gtrsim 4n_0$, respectively.

in turn, as a (possibly measurable) shift to higher values of the frequency of gravitational waves (GWs) emitted from the merged object [5–11]. A too large reduction of the stellar radius, however, is disfavored by the recent the neutron star interior composition explorer mission (NICER) observations and analyses, reporting similar radii for NSs with masses of 1.4 $M_\odot$ and 2.1 $M_\odot$ [12–15].

An alternative to a 1PT is a continuous crossover from hadronic matter to quark matter. Some of the present authors constructed quark-hadron-crossover (QHC) EOS [16–19], generally finding a peak in the sound speed, $c_s/c = \sqrt{dP/de}$, exceeding the conformal limit $c/\sqrt{3}$, with c being the speed of light; see Fig. 2. Microscopic considerations on the structure of such a peak [20,21] emphasize the importance of quark substructure in baryons and of quark Pauli blocking effects. Peaks in sound speed are absent in EOS involving 1PTs or in purely hadronic models. In the latter, stiffening results from nuclear many-body repulsions, which keep growing with density, leading to monotonic growth in sound speed. The existence of a peak in sound speed in QHC EOS is unique and can be taken as the signature for the onset of quark-matter formation.

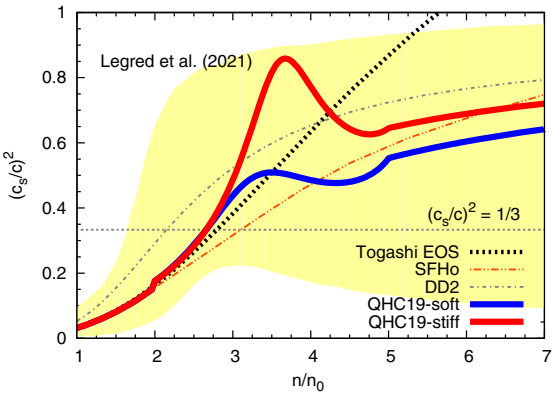

FIG. 2. Square of sound speed normalized to the speed of light, $c_s^2/c^2 = dP/de$, for our QHC EOS with soft and stiff sets of quark model parameters and for representative hadronic EOS: Togashi EOS [22], SFHo [23], and DD2 [24]. The yellow band is the allowed region in the model-agnostic approach of Legred *et al.* [25] (see also [26]). The conformal limit, $c_s^2 = c^2/3$, which should be reached in the high-density limit, is also shown as a guide.

In this Letter, for the first time, results of numerical simulations of BNS mergers with EOS based on QHC are reported. We adopt the QHC19 EOS [18], which is based on the Togashi nucleonic EOS [22] for $n \leq 2n_0$ and a pure quark EOS for $n \gtrsim 5n_0$, with the crossover region calculated through interpolation [18]. We compare results with simulations adopting the Togashi EOS over the whole density range. The QHC19 and Togashi EOS differ substantially only for $n \gtrsim 3n_0$, and, since the maximum values of n in our inspiraling NSs are around $3n_0$ (cf. Fig. 3), the properties (like tidal deformability [27,28]) of stars built with the above different EOS and their dynamics (like the evolution of the central number density or of the GW frequency) during the inspiral differ by less than 1% (see Table 1 in the Supplemental Material [29]). More remarkable differences are expected only during and after the merger.

Numerical setup.—As a first step to explore the role of a QHC in BNS mergers, we focus on equal-mass configurations, and, with the goal of studying postmerger dynamics, we chose four relatively low-mass models, in which the gravitational masses of each NS at infinite separation are $M/M_\odot = 1.250$, 1.300, 1.350, and 1.375. We refer to these as M1.25, M1.30, M1.35, M1.375, respectively. The last

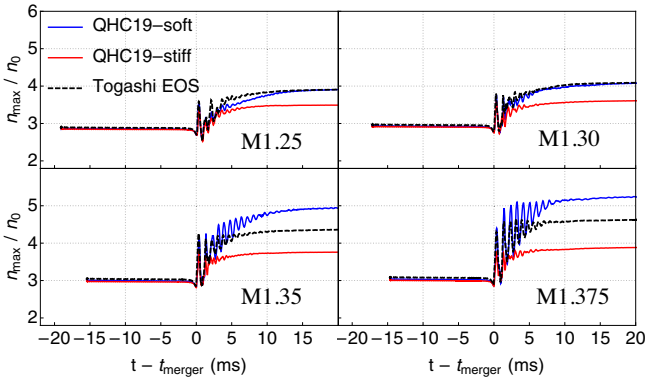

FIG. 3. Evolution of the maximum number density for simulations employing the QHC19 and Togashi EOS with different initial masses. $t_{\rm merger}$ is the merger time defined as the time of the maximum amplitude of $|h| \equiv (h_+^2 + h_\times^2)^{1/2}$.

5–7 orbits are simulated for the different models, all starting from the same orbital separation.

We performed fully general-relativistic simulations adopting two QHC models, QHC19B (named here QHC19-stiff), QHC19D (named QHC19-stiff) [18], and the purely hadronic Togashi EOS [22]. Additional description of the EOS, the codes, the NS properties, and some of the numerical parameters used in our simulations is presented in the Supplemental Material [29]. Here, we briefly comment only on how we mimic thermal effects in matter, even when adopting an EOS, like QHC19, that does not contemplate them. Ours is a standard treatment in numerical relativity, but we discuss it nevertheless because it may be of interest to a wider audience. Approximate thermal effects are included by adding to the pressure given by the *cold* EOS a component calculated by assuming an *ideal-gas* behavior with a constant ideal-gas index $\Gamma_{\rm th}$, chosen in the range 1.5–2.0 to reproduce realistic values (see, e.g., [30–38]). Note that the lifetime before collapse to black hole of the material object formed in the merger depends also on thermal support and thus on the *ad hoc* value of $\Gamma_{\rm th}$, but postmerger oscillation frequencies (see below) are relatively insensitive to it [39]. The lifetime before collapse is a quantity that anyway cannot currently be estimated accurately in numerical simulations, because it depends sensitively on many factors, including nonphysical ones like grid setup and resolution. We focus, instead, on postmerger oscillation frequencies and, in order to have higher power in the oscillation modes, we chose the highest reasonable value, $\Gamma_{\rm th} = 2$, which gives the longest lifetime before collapse. See Sec. IV of the Supplemental Material for details [29].

Results and discussion.—As seen in Fig. 2, both QHC19-soft and QHC19-stiff are stiffer (have higher sound speed) than the Togashi EOS at densities slightly above $2n_0$. The Togashi EOS is stiffer than QHC19-soft for $n \gtrsim 3.5n_0$ and stiffer than QHC19-stiff for $n \gtrsim 4.0n_0$. Within the density range reached in our BNS simulations (cf. Fig. 3), QHC19-stiff is thus always stiffer than the Togashi EOS for all models with different masses considered here, while QHC19-soft is softer, in some regions, for high-mass BNSs.

In QHC19-stiff, the sound speed (and thus pressure support) around $3.5n_0$ increases the most; it is then expected that inspiraling stars and merged objects in BNSs with QHC19-stiff are less compact than those with the Togashi or QHC19-soft EOS, as can be ascertained in Fig. 3: the maximum number density $n_{\rm max}(t)$ is smaller than for the other EOS, in the inspiral, after the merger, and (on average) during the merger. Even in our most massive case, $n_{\rm max}$ for QHC19-stiff reaches up only to $\approx 3.8n_0$. At such densities, indeed, stiffening due to the crossover is still important.

In QHC19-soft, in contrast, the evolution of $n_{\rm max}$ is different for binaries of different masses. Since for densities $\lesssim 3.5n_0$ QHC19-soft is stiffer than the Togashi EOS, in our lowest-mass case, M1.25, in which densities higher than $3.5n_0$ are reached only toward the end of our simulations, we see that $n_{\rm max}$ is always smaller than that for the Togashi EOS. For M1.30, where the maximum density after the merger reaches 3.5–$4n_0$, the differences between the QHC19-soft and Togashi EOS appear to average out (their sound-speed curves cross around $3.5n_0$; cf. Fig. 2), leading to similar evolution. For even larger masses, M1.35 and M1.375, during and after the merger, densities greater than $\sim 3.5n_0$ are reached in a wide region, and hence QHC19-soft leads to a considerably more compact merged object.

The oscillations of the merged object produce intense GW emission, characterized by distinct peaks in the power spectrum, whose frequencies are found to correlate with stellar properties like compactness, average density, or tidal deformability [39–44]. At least three peaks (f_1, f_2, and f_3, sometimes referred to with different names in the literature) may be identified in most cases, but basically only one, f_2, is not transient and remains even after a few milliseconds [2,45–50]. The f_2 frequency slightly changes in time, as the density profile changes because of GW emission and angular-momentum transfer from inner parts to outer parts [51].

Figure 4 displays the fundamental and dominant harmonic mode ($\ell = m = 2$) of the plus polarization of the GW strain h_+^{22} for the M1.35 configurations (top panels) and the corresponding time-frequency evolution and instantaneous frequency (bottom panels). Some similarities and differences between our purely hadronic and QHC models are apparent. The damping times for postmerger GWs (signaled by the extinguishing of the red color over the whole frequency band in the spectrogram) are seen to be dependent on the EOS, and the time interval in which a wide range of frequencies has a lot of power (the time interval in which the spectrogram has a bright band) is shorter for QHC19-stiff. This means that the transient period between the merger and the time when gravitational radiation settles to a well-identified main frequency, f_2, is shorter for QHC19-stiff.

We also note that, in all our simulations (with and without a QHC), the instantaneous frequency in the late postmerger phase after the transient period approximately approaches a constant, though a different one for different models. This is in contrast with hybrid EOS models with 1PTs that predict an abrupt decrease in pressure support, causing the object to shrink rapidly and thus an increase of the instantaneous GW frequency [5–11].

To estimate quantitatively the peak frequencies together with their uncertainties, we employ a Markov Chain Monte Carlo fitting method [52] based on Bayesian inference [53]. We fit the f_1 peak with a Gaussian model and the f_2 peak with a model that considers skewness. The latter has been chosen to describe the decay of the mode and the frequency shift during the transient phase [39,45] (see also Sec. III of the Supplemental Material [29]).

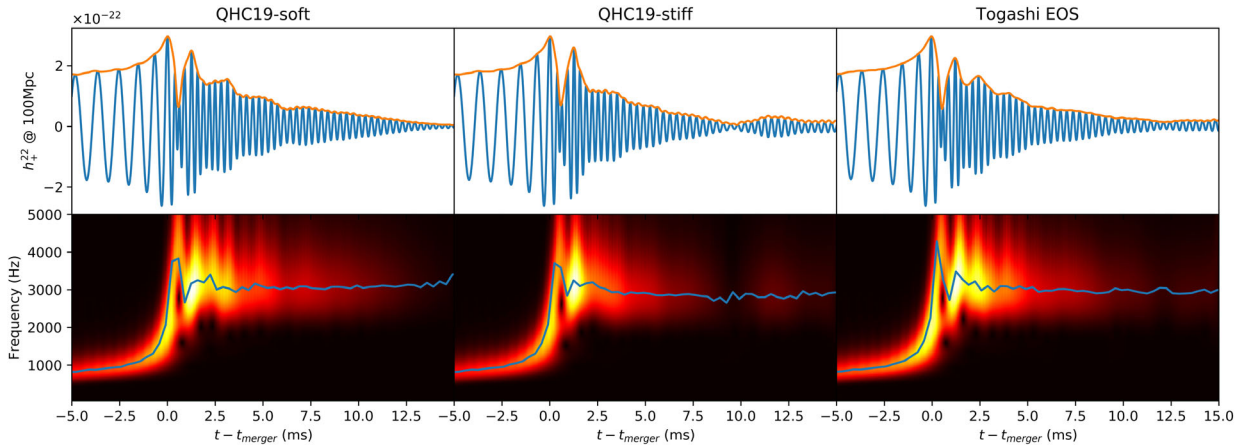

FIG. 4. Top: fundamental and dominant harmonic mode ($\ell = m = 2$) of the plus polarization of the GW strain with amplitude envelope for the M1.35 models. Bottom: spectrogram (brighter colors indicate higher power in the spectrum) and instantaneous frequency of the same models.

As is well known, the relations between the values of f_2 in different configurations are similar to the respective relations between the values of $n_{\max}$ (on average) since postmerger frequencies are related to compactness or average density [39–44], but comparing the values of f_2 for different EOS and BNS masses gives important clues on how to discriminate observationally different types of quark dynamics in the high-density end of EOS. Figure 5 shows the fitting results of f_2 for different EOS and binary masses, with their 68% fitting uncertainty range, which is comparable to the numerical accuracy of our simulations (see Sec. II of the Supplemental Material [29]).

For all masses, f_2 for QHC19-stiff is lower than that for the Togashi EOS, and this is related to the lower compactness of the merged object, which is, in turn, related to the pronounced peak in sound speed for QHC19-stiff. For QHC19-soft, except for our lowest-mass case, f_2 is higher than that for the Togashi EOS. In models M1.25, f_2 for both QHC19-soft and QHC19-stiff is lower than that for the Togashi EOS. This is because quark-matter densities ($\sim 5n_0$), where the QHC EOS are softer than the Togashi EOS, are not reached, and thus the remnant is less compact. This is a unique feature of the peak in sound speed present in QHC models and is independent of the height of such peak (namely, of the parameters of the specific QHC EOS). Note, however, that, since the stiffening in the crossover domain is strongly affected by the quark-matter EOS it is attached to, even in lower-mass models one may still, in principle, gain from observations useful information on how quarks are liberated in high-density hadronic matter.

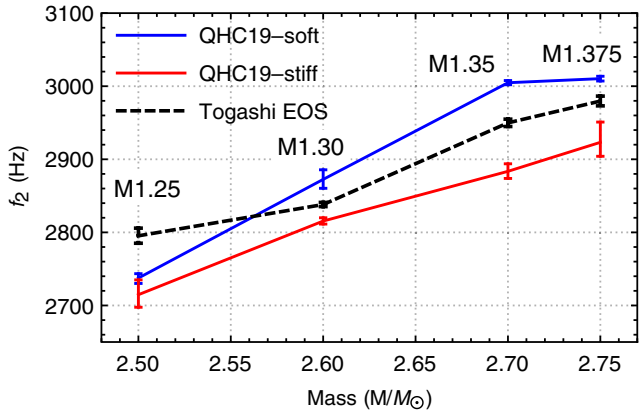

FIG. 5. Relation between f_2 and the total mass of the binary.

In order to study further whether it may be possible to discriminate observationally between EOS with a QHC or with a 1PT, we define Δf_2 as the difference between the f_2 resulting from an EOS with a 1PT or crossover and the f_2 resulting from its baseline EOS: $\Delta f_2 \equiv f_2^{\text{phase transition or crossover}} - f_2^{\text{baseline}}$.

For the QHC EOS employed here, Δf_2 is in the range $\pm(50\text{–}100)$ Hz and, more importantly, is negative for all QHC19-stiff models and for the lower-mass model of QHC19-soft. This is in contrast to the case of EOS with a 1PT, in which Δf_2 is always found to be positive in the literature (see also Sec. V of the Supplemental Material [29]). This is a qualitative feature that makes it relatively simple to discriminate observationally between these different types of EOS. In particular, an observation of a low-mass BNS system, such as our M1.25 model, would allow one to distinguish between QHC EOS and EOS with a 1PT, according to the sign of the measured Δf_2.

For higher masses and for (weak) 1PTs that result in a Δf_2 comparable to that of QHC EOS, it may be difficult to discriminate from observations, unless the 1PT occurs some time after the merger. In this case, the value of f_2 would change abruptly [8] and, if this change can be measured, it would be a clear difference with respect to QHC EOS (cf. Fig. 4).

Conclusions.—In this Letter, we performed the first (and fully general-relativistic) simulations of BNS mergers with

EOS based on QHC (QHC19) and discussed how they could be distinguished from purely hadronic EOS or hybrid quark-hadron EOS with 1PTs.

We found that a QHC EOS with a pronounced peak in sound speed, like QHC19-stiff, leaves a clear and unique signature in the postmerger main frequency: for any binary mass, f_2 is lower than that of the baseline hadronic EOS, and thus also lower than that expected for EOS with a 1PT. In higher-mass mergers with the QHC19-soft EOS, instead, it may be difficult to discriminate from a weak 1PT, unless the value of f_2 is observed to change rapidly in time, a signature of a 1PT occurring after the merger [8].

Results of this Letter will become relevant to observations when GWs in the kilohertz band are surveyed with higher sensitivity by an upgraded Advanced Laser Interferometer Gravitational Wave Observatory (LIGO) (A+ [54]) and third-generation observatories (e.g., the Einstein Telescope [55] and Cosmic Explorer [56]), also with a specifically optimized design (e.g., Neutrino Ettore Majorana Observatory (NEMO) [57]).

In fact, sensitivities on the order of 50 Hz in this band, sufficient to distinguish a QHC EOS from a purely hadronic one, are estimated to be reached in these detectors. For example, Ref. [58] estimated that f_2 can be measured to within about 36 (27){45} Hz at the 90% credible level for a stiff (moderate) {soft} EOS at a postmerger signal-to-noise ratio of 5. Other works make similar predictions, for signal-to-noise ratio $\gtrsim$10 [59]. A signal-to-noise ratio $\gtrsim$5–10 is predicted to be attainable easily for sources at 200 Mpc or even more by Cosmic Explorer [60] and Einstein Telescope [55], leading to reasonably frequent measurements.

This work is a first attempt to study in BNS mergers the unique features of QHC EOS. We plan to extend the analysis in several directions, first by adopting the QHC21 [19] EOS, which improves further over QHC19 under the microscopical point of view and which was made public after we finished our simulations. We will explore the relationship between some EOS parameters and observable quantities, as well as finite-temperature effects, expected to be important for the onset of quark saturation [21]. We also plan to perform simulations of unequal-mass binaries and study the influence of QHC EOS on mass ejecta.

This work is supported in part by the Japan Society for the Promotion of Science (JSPS; KAKENHI Grants No. JP19H00693, No. JP19KK0354, No. JP20H04753, No. JP21H01088, No. T18K03622, No. JP17K14305, No. JH18H03712, and No. JH18H05236), by the Pioneering Program of RIKEN for Evolution of Matter in the Universe (r-EMU), by the Graduate Program on Physics for the Universe at Tohoku University, and by the National Natural Science Foundation of China (No. 11933010, No. 11875144, and No. 12233011). Simulations were performed on the Hokusai supercomputer at RIKEN, on the Aterui II supercomputer (Cray XC50) at the Center for Computational Astrophysics of NAOJ, and on the BSCC-M supercomputer at the Beijing Super Cloud Computing Center.

*Corresponding author.
huangyj@pmo.ac.cn

[1] B. P. Abbott *et al.* (LIGO Scientific, Virgo Collaborations), Phys. Rev. Lett. **119**, 161101 (2017).
[2] L. Baiotti, Prog. Part. Nucl. Phys. **109**, 103714 (2019).
[3] G. F. Burgio, H. J. Schulze, I. Vidaña, and J. B. Wei, Prog. Part. Nucl. Phys. **120**, 103879 (2021).
[4] E. Fonseca *et al.*, Astrophys. J. Lett. **915**, L12 (2021).
[5] A. Bauswein, N.-U. F. Bastian, D. B. Blaschke, K. Chatziioannou, J. A. Clark, T. Fischer, and M. Oertel, Phys. Rev. Lett. **122**, 061102 (2019).
[6] E. R. Most, L. J. Papenfort, V. Dexheimer, M. Hanauske, S. Schramm, H. Stöcker, and L. Rezzolla, Phys. Rev. Lett. **122**, 061101 (2019).
[7] E. R. Most, L. Jens Papenfort, V. Dexheimer, M. Hanauske, H. Stoecker, and L. Rezzolla, Eur. Phys. J. A **56**, 59 (2020).
[8] L. R. Weih, M. Hanauske, and L. Rezzolla, Phys. Rev. Lett. **124**, 171103 (2020).
[9] S. Blacker, N.-U. F. Bastian, A. Bauswein, D. B. Blaschke, T. Fischer, M. Oertel, T. Soultanis, and S. Typel, Phys. Rev. D **102**, 123023 (2020).
[10] S. L. Liebling, C. Palenzuela, and L. Lehner, Classical Quantum Gravity **38**, 115007 (2021).
[11] A. Prakash, D. Radice, D. Logoteta, A. Perego, V. Nedora, I. Bombaci, R. Kashyap, S. Bernuzzi, and A. Endrizzi, Phys. Rev. D **104**, 083029 (2021).
[12] M. C. Miller *et al.*, Astrophys. J. Lett. **918**, L28 (2021).
[13] T. E. Riley *et al.*, Astrophys. J. Lett. **918**, L27 (2021).
[14] G. Raaijmakers, S. K. Greif, K. Hebeler, T. Hinderer, S. Nissanke, A. Schwenk, T. E. Riley, A. L. Watts, J. M. Lattimer, and W. C. G. Ho, Astrophys. J. Lett. **918**, L29 (2021).
[15] M.-Z. Han, Y.-J. Huang, S.-P. Tang, and Y.-Z. Fan, arXiv:2207.13613.
[16] K. Masuda, T. Hatsuda, and T. Takatsuka, Astrophys. J. **764**, 12 (2013).
[17] G. Baym, T. Hatsuda, T. Kojo, P. D. Powell, Y. Song, and T. Takatsuka, Rep. Prog. Phys. **81**, 056902 (2018).
[18] G. Baym, S. Furusawa, T. Hatsuda, T. Kojo, and H. Togashi, Astrophys. J. **885**, 42 (2019).
[19] T. Kojo, G. Baym, and T. Hatsuda, Astrophys. J. **934**, 46 (2022).
[20] L. McLerran and S. Reddy, Phys. Rev. Lett. **122**, 122701 (2019).
[21] T. Kojo, Phys. Rev. D **104**, 074005 (2021).
[22] H. Togashi, K. Nakazato, Y. Takehara, S. Yamamuro, H. Suzuki, and M. Takano, Nucl. Phys. **A961**, 78 (2017).
[23] A. W. Steiner, M. Hempel, and T. Fischer, Astrophys. J. **774**, 17 (2013).
[24] S. Typel, G. Röpke, T. Klähn, D. Blaschke, and H. H. Wolter, Phys. Rev. C **81**, 015803 (2010).
[25] I. Legred, K. Chatziioannou, R. Essick, S. Han, and P. Landry, Phys. Rev. D **104**, 063003 (2021).

[26] M.-Z. Han, J.-L. Jiang, S.-P. Tang, and Y.-Z. Fan, Astrophys. J. **919**, 11 (2021).
[27] T. Hinderer, Astrophys. J. **677**, 1216 (2008).
[28] T. Hinderer, Astrophys. J. **697**, 964 (2009).
[29] See Supplemental Material at http://link.aps.org/supplemental/10.1103/PhysRevLett.129.181101 for details on the models, the numerical code and setup, the fitting procedures, and the equations of state used.
[30] A. Bauswein, H.-T. Janka, and R. Oechslin, Phys. Rev. D **82**, 084043 (2010).
[31] L. Rezzolla and O. Zanotti, *Relativistic Hydrodynamics* (Oxford University Press, Oxford, United Kingdom, 2013).
[32] H. Togashi, M. Takano, K. Sumiyoshi, and K. Nakazato, Prog. Theor. Exp. Phys. **2014**, 023D05 (2014).
[33] J.-J. Lu, Z.-H. Li, G. F. Burgio, A. Figura, and H. J. Schulze, Phys. Rev. C **100**, 054335 (2019).
[34] A. Figura, J.-J. Lu, G. F. Burgio, Z.-H. Li, and H. J. Schulze, Phys. Rev. D **102**, 043006 (2020).
[35] S. Huth, C. Wellenhofer, and A. Schwenk, Phys. Rev. C **103**, 025803 (2021).
[36] C. A. Raithel, V. Paschalidis, and F. Özel, Phys. Rev. D **104**, 063016 (2021).
[37] A. R. Raduta, F. Nacu, and M. Oertel, Eur. Phys. J. A **57**, 329 (2021).
[38] J. Keller, C. Wellenhofer, K. Hebeler, and A. Schwenk, Phys. Rev. C **103**, 055806 (2021).
[39] K. Takami, L. Rezzolla, and L. Baiotti, Phys. Rev. D **91**, 064001 (2015).
[40] L. Baiotti, B. Giacomazzo, and L. Rezzolla, Phys. Rev. D **78**, 084033 (2008).
[41] A. Bauswein and H.-T. Janka, Phys. Rev. Lett. **108**, 011101 (2012).
[42] K. Hotokezaka, K. Kiuchi, K. Kyutoku, T. Muranushi, Y.-i. Sekiguchi, M. Shibata, and K. Taniguchi, Phys. Rev. D **88**, 044026 (2013).
[43] K. Takami, L. Rezzolla, and L. Baiotti, Phys. Rev. Lett. **113**, 091104 (2014).
[44] S. Bernuzzi, T. Dietrich, and A. Nagar, Phys. Rev. Lett. **115**, 091101 (2015).
[45] L. Rezzollaand K. Takami, Phys. Rev. D **93**, 124051 (2016).
[46] A. Bauswein, N. Stergioulas, and H.-T. Janka, Eur. Phys. J. A **52**, 56 (2016).
[47] A. Bauswein and N. Stergioulas, J. Phys. G **46**, 113002 (2019).
[48] J. L. Friedman and N. Stergioulas, Int. J. Mod. Phys. D **29**, 2041015–632 (2020).
[49] S. Bernuzzi, Gen. Relativ. Gravit. **52**, 108 (2020).
[50] T. Dietrich, T. Hinderer, and A. Samajdar, Gen. Relativ. Gravit. **53**, 27 (2021).
[51] M. Hanauske, K. Takami, L. Bovard, L. Rezzolla, J. A. Font, F. Galeazzi, and H. Stöcker, Phys. Rev. D **96**, 043004 (2017).
[52] D. Foreman-Mackey, D. W. Hogg, D. Lang, and J. Goodman, Publ. Astron. Soc. Pac. **125**, 306 (2013).
[53] A. Gelman, J. B. Carlin, H. S. Stern, and D. B. Rubin, *Bayesian Data Analysis*, 2nd ed. (Chapman and Hall/CRC, Boca Raton, 2004).
[54] J. Miller, L. Barsotti, S. Vitale, P. Fritschel, M. Evans, and D. Sigg, Phys. Rev. D **91**, 062005 (2015).
[55] M. Punturo *et al.*, Classical Quantum Gravity **27**, 194002 (2010).
[56] B. P. Abbott *et al.*, Classical Quantum Gravity **34**, 044001 (2017).
[57] K. Ackley *et al.*, Pub. Astron. Soc. Aust. **37**, e047 (2020).
[58] K. Chatziioannou, J. A. Clark, A. Bauswein, M. Millhouse, T. B. Littenberg, and N. Cornish, Phys. Rev. D **96**, 124035 (2017).
[59] M. Breschi, S. Bernuzzi, F. Zappa, M. Agathos, A. Perego, D. Radice, and A. Nagar, Phys. Rev. D **100**, 104029 (2019).
[60] V. Srivastava, D. Davis, K. Kuns, P. Landry, S. Ballmer, M. Evans, E. D. Hall, J. Read, and B. S. Sathyaprakash, Astrophys. J. **931**, 22 (2022).